Pure Appl. Chem., Vol. 80, No. 6, pp. 1337–1347, 2008.
doi:10.1351/pac200880061337

On the solvent role in alcohol-induced α-helix formation of chymotrypsin inhibitor 2*

Koji Yoshida, Junko Kawaguchi, Sannum Lee, and Toshio Yamaguchi‡

Advanced Materials Institute and Department of Chemistry, Faculty of Science, Fukuoka University, Nanakuma, Jonan-ku, Fukuoka 814-0180, Japan

Abstract: The circular dichroism (CD) spectra of chymotrypsin inhibitor 2 (CI2) have been measured as a function of alcohol mole fraction in aqueous mixtures of methanol, ethanol, trifluoroethanol (TFE), and hexafluoro-iso-propanol (HFIP). Small-angle X-ray and neutron scattering (SAXS and SANS) of CI2 was also measured as a function of ethanol mole fraction in ethanol–water mixtures. The CD spectra have shown that the secondary structure of CI2 changes from β-strand to α-helical structure at alcohol mole fractions characteristic of the individual alcohols in an order of HFIP > TFE > ethanol > methanol in effectiveness, where the structure transition of solvent clusters takes place from the typical tetrahedral-like water to the chain-like alcohol clusters in alcohol–water mixtures previously reported. The radius of gyration of CI2, obtained from the analysis of the SANS data, increased with an increase in ethanol mole fraction up to around 0.2 and then gradually decreased. The SAXS data have shown that the shape of CI2 changes from a sphere to a rod-like one at a 0.1 ethanol mole fraction. A possible role of solvent clusters played in alcohol-induced α-helix formation of CI2 is discussed from a viewpoint of the solvent clusters.

Keywords: chymotrypsin inhibitor 2; alcohol–water mixture; small-angle X-ray scattering; small-angle neutron scattering; α-helix formation; solvent clusters.

INTRODUCTION

Alcohol-induced α-helix formation of peptides and proteins is well known and has been widely used in biophysics and biochemistry [1]. A number of experimental studies on the secondary structure of peptides and proteins in various alcohol–water mixtures have been carried out extensively [2–8]; among various alcohols, fluoroalcohols, such as 2,2,2-trifluoroethanol (TFE) and 1,1,1,3,3,3-hexafluoro-iso-propanol (HFIP), have been found to be more effective than aliphatic alcohols in stabilizing the α-helical structure of peptides and proteins; e.g., HFIP is about 20 times more effective than methanol in the denaturation of β-lactoglobulin and the α-helix formation of melittin [8]. The solvent effect on α-helix formation of peptides and proteins has long been discussed in terms of electrostatic interactions by treating medium as a dielectric continuum; however, Hong et al. [8] have shown in their circular dichroism (CD) spectral measurements of β-lactoglobulin and melittin in aqueous mixtures of methanol, ethanol, TFE, and HFIP that α-helix formation of the proteins cannot be explained in terms of dielectric constants of the solvents and suggested that solvents play an important role at a molecular level in

*Paper based on a presentation at the 30th International Conference on Solution Chemistry (ICSC 30), 16–20 July 2007, Perth, Australia. Other presentations are published in this issue, pp. 1195–1347.

‡Corresponding author: E-mail: yamaguch@fukuoka-u.ac.jp, Tel.: +81-92-871-6631 ext. 6224, Fax: +81-92-865-6030

changing the secondary structure of the peptides. Thus, the underlying mechanism of alcohol-induced α-helix formation of peptides and proteins still remains an open question at a molecular level, and a new molecular approach to this problem is highly needed.

Kinoshita et al. [9] used a reference interaction site model (RISM) theory to calculate the thermodynamic properties of various conformations of Met-enkephalin and C-peptide fragment of ribonuclease A in methanol, ethanol, and water. Their results showed that alcohols facilitate the peptide molecules to form the α-helical structure by forming intramolecular hydrogen bonds in alcohols. They concluded that the solvation free energy of the peptides in alcohols becomes less dependent on the conformational change than in water because of smaller solvation number of the peptide in alcohols than that in water, and that the conformational stability in alcohols is governed mostly by the conformational energy. Fioroni et al. [10] studied solvation phenomena of a tetrapeptide in water–TFE and water–ethanol mixtures by NMR and molecular dynamics (MD) simulation and revealed preferential solvation on the surface on the peptide by TFE in the water–TFE mixtures, but not by ethanol in the water–ethanol mixtures. We have performed a replica-exchange molecular dynamics (REMD) simulation on a 10-residue model peptide in water and in ethanol that were treated explicitly and found that the peptide tends to form a more compact structure in ethanol than in water due to intramolecular hydrogen bonding within the peptide in ethanol [11]. However, none of the above approaches have been based on solvent structures.

In recent years, an advanced X-ray diffraction technique with an imaging plate as an area detector and neutron diffraction with isotopic substitution (NDIS) method combined with molecular simulation (empirical potential structure refinement, EPSR) have enabled us to determine the detailed structure of aqueous mixtures of methanol [12], ethanol [13–15], TFE [16], and HFIP [17,18] as a function of alcohol concentration at a molecular level. The results of these studies have demonstrated that structural transition of solvent clusters takes place at specific alcohol concentrations depending on the nature of the hydrophobic groups of alcohols. Interestingly, the specific alcohol concentrations of the structural transition are consistent with those where anomalies in various physicochemical properties are observed for alcohol–water mixtures.

In this study, chymotrypsin inhibitor 2 (CI2) that has both α-helix and β-sheet structures is synthesized, and the CD spectra of CI2 are measured as a function of alcohol mole fractions in aqueous solutions of methanol, ethanol, TFE, and HFIP to investigate the effect on various alcohols on the secondary structure of CI2. Moreover, the size and shape of CI2 are determined as a function of alcohol mole fraction in ethanol–water mixtures by small-angle X-ray and neutron scattering methods (SAXS and SANS). A possible mechanism in alcohol-induced α-helix formation of CI2 in various alcohol–water mixtures is discussed from a structure point of view of solvent clusters.

EXPERIMENTAL

Synthesis of CI2

CI2 (64 residues) has one α-helix and six β-strands which form four β-sheets. The amino sequence of CI2 is LKTEWPELVG KSVEEAKKVI LQDKPEAQII VLPVGTIVTM EYRIDRVRLF VDKLDIAQVP RVG [19–21]. Peptides were synthesized by the solid-phase method using fluorenylmethoxycarbonyl (Fmoc) chemistry on a Pioneer Peptide Synthesis System (Perspective Biosystems). Fmoc-Gly-PEG-PS resins (Perspective Biosystems) were used for all coupling reactions, where the activation reagent HATU, *O*-(7-azabenzotriazole-1-yl)-*N*,*N*,*N*′*N*′-tetramethyluronium hexafluorophosphate, was used. The peptide-bound resins were treated by 2,2,2-trifluoroacetic acid (22.5 ml) containing *m*-cresol (0.6 ml), ethandithiol (1.8 ml), and thioanisole (3.5 ml) for 1.5 h at room temperature. The crude peptides obtained were treated with Sephadex G-25 column (25 mm × 130 cm). Then the peptide was purified on a preparative C18 reverse-phase high-performance liquid chromatography (RP-HPLC). Peptide purities were confirmed by analytical RP-HPLC and matrix-assisted laser desorp-

tion ionization with time-of-flight mass spectrometry (MALDI-TOF) (Voyager-DE STR, Perspective Biosystems). The peptide concentrations were determined from UV-absorbance of Trp at 280 nm ($\varepsilon = 5500$ mol^{-1} cm^{-1}) in water.

CD measurements

Methanol (purity 99.5 %), ethanol (99.5 %), and HFIP (99.0 %) purchased from Wako Pure Chemical Industries, and TFE (99.5 %) from Aldrich were used without further purification. The peptide stock solutions of ~1 mM were prepared by dissolving CI2 into triple-distilled water (Milli-Q Plus, Millipore Japan) and their concentrations were determined by measuring tyrosine absorbance at 280 nm on FT-210 UV spectrophotometer (JASCO). The sample peptide solutions were prepared by mixing the stock peptide solutions, triple-distilled water, and respective alcohols to alcohol mole fractions of 0~0.6 for methanol and ethanol, 0~0.35 for TFE, and 0~0.3 for HFIP, and of peptide concentrations of 25 and 40 μM for far-UV and near-UV CD spectral measurements, respectively, on a J-600 spectrometer (JASCO). Quartz cells with 0.1- and 1.0-cm path lengths were used for far-UV and near-UV CD measurements, respectively. Four scans were accumulated for each measurement. The least-squares fitting analysis of secondary structures was performed over a wavelength of 196~260 nm with the program SELCOM3 [22].

SAXS measurements

The peptide sample solutions were prepared as described in the previous section so that the peptide concentration was 400 μM and ethanol mole fractions were 0~0.4. The solutions were inserted into stainless steel cells with mica windows (thickness less than 15 μm). SAXS measurements were made at 298 ± 0.1 K on the peptide solutions, the corresponding solvents alone, empty cell, and background at BL-10C in the Photon Factory of the National Laboratory for High Energy Accelerator Research Organization (KEK). The wavelength used was 1.488 Å produced from a double Si(111) crystal monochromator. The sample-detector distance was 90 cm, corresponding to an accessible q ($= 4\pi/\lambda \sin\theta$, λ is the wavelength and 2θ is the scattering angle) range of 0.044~0.3 Å^{-1}. The PSPC detector was calibrated against the sixth-order scattering of dried collagen of hen tendon as a standard. The time of measurements was 10 min for each sample to prevent decomposition of peptides by irradiation. The scattering intensities of the samples and the solvents were corrected for absorption, and the contributions from CI2 were obtained by subtracting the solvent scattering from those of the CI2 solutions.

SANS measurements

D_2O (D content 99.8 %) was purchased from Merck, and C_2D_5OD (99.6 %) from CDN Isotopes. Peptide sample solutions were prepared by mixing the CI2 stock solution, D_2O, and C_2D_5OD to a peptide concentration of 400 μM and ethanol mole fractions of 0~0.4 in a nitrogen-filled glove box. The sample solutions were inserted into rectangular quartz cells of 12 mm in width, 20 mm in height, and 2 mm in sample thickness. SANS measurement was made on the small-angle neutron spectrometer SWAN at the spallation neutron facility (KENS) of KEK. The sample-detector distance was 3.3 m. The wavelengths of cold neutrons used were 1–16 Å, corresponding to the scattering vector q-range = 0.1~10 Å^{-1}. The neutron beam size at the sample position was 10 × 10 mm. The accumulated time was 6–7 h per sample. The SANS spectra were collected for aqueous ethanol solutions of CI2 as a function of ethanol mole fraction. The solvent-mixtures and empty cells were also measured. All the data were corrected for absorption by using the transmission data measured. The SANS data of CI2 alone were obtained after subtraction of the spectra of the solvents from those of the CI2 samples.

RESULTS

CD spectra

Figure 1 shows the far-UV CD spectra of CI2 in aqueous mixtures of methanol, ethanol, TFE, and HFIP as a function of alcohol mole fraction. The far-UV CD spectrum of CI2 in pure water shows that CI2 takes mostly β-sheet and random structures. With increasing alcohol mole fraction, two negative peaks grow at around 208 and 222 nm, showing the formation of α-helix structure in all alcohol–water mixtures. The least-squares fitting analysis of the secondary structure was performed by taking into account α-helix, β-strand, turns, and unordered structure for the far-UV CD spectra over a wavelength range of 196–260 nm. The fractions of the individual components finally obtained are plotted against an alcohol mole fraction for CI2 in all alcohol–water mixtures in Fig. 2.

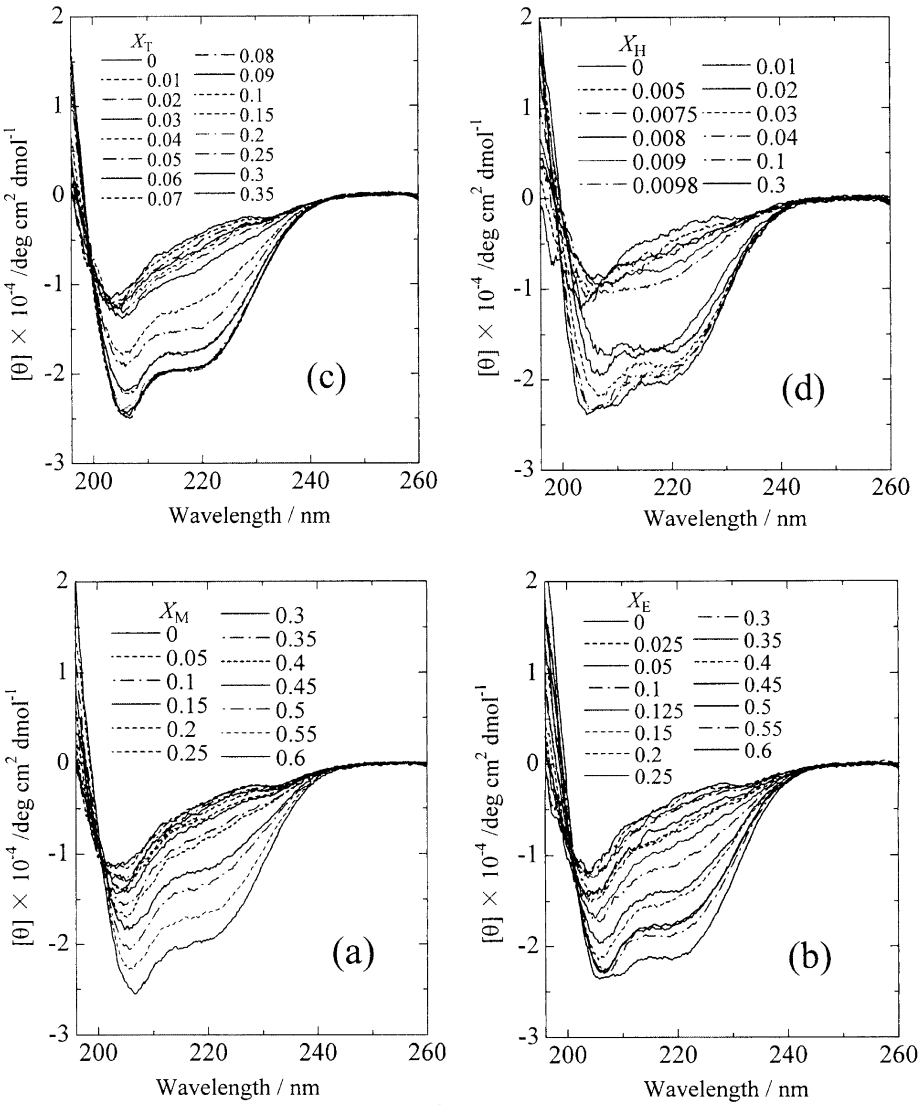

Fig. 1 Far-UV CD spectra of CI2 in aqueous mixtures of methanol (a), ethanol (b), TFE (c), and HFIP (d) as a function of alcohol mole fraction.

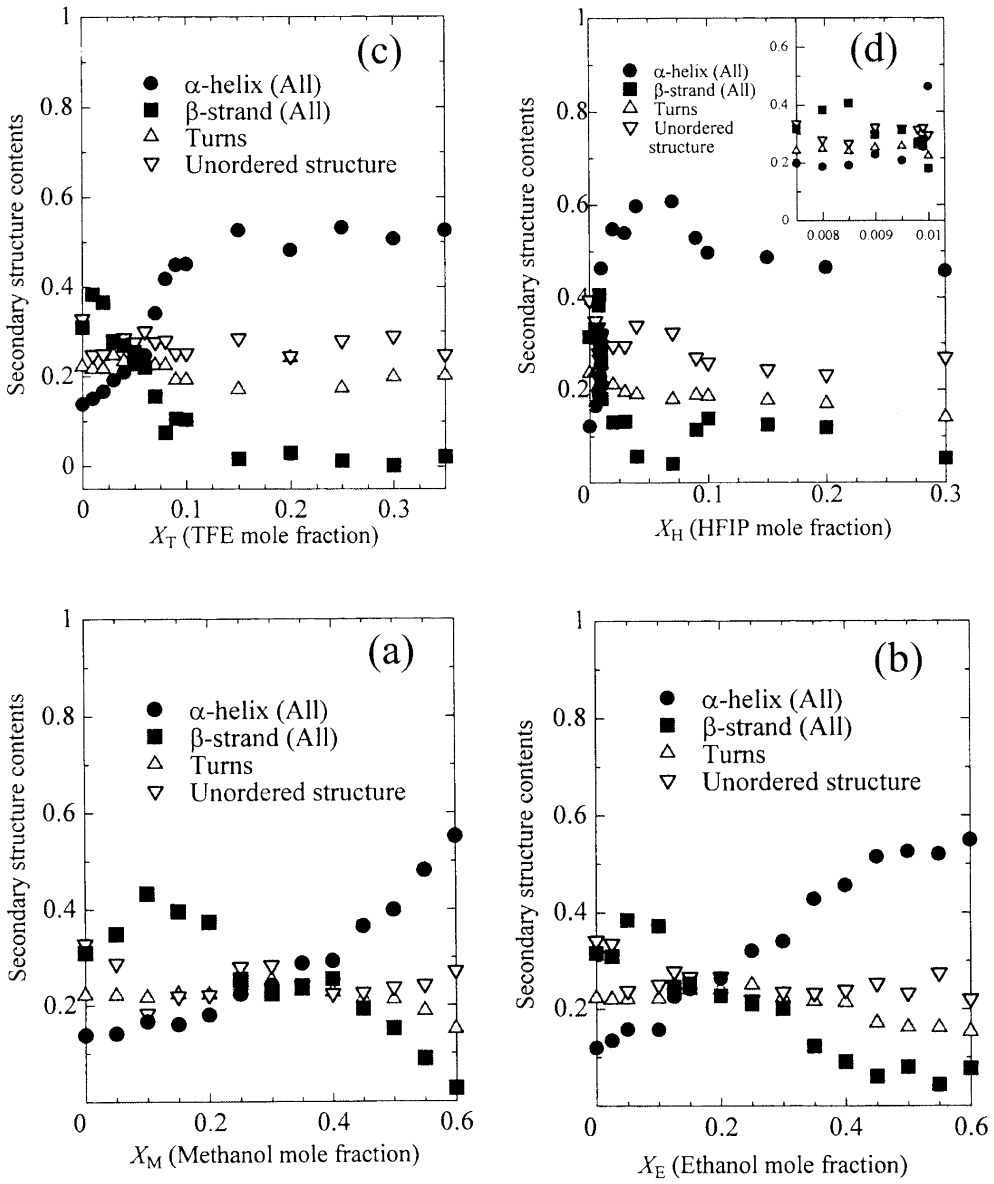

Fig. 2 Fractions of the secondary structure of CI2 in aqueous mixtures of methanol (a), ethanol (b), TFE (c), and HFIP (d) as a function of alcohol mole fraction.

In methanol–water mixture, the fraction of β-strand structure had a maximum at ~0.1 of methanol mole fraction (x_M) and then decreased with increasing x_M. On the other hand, the fraction of α-helix did not change appreciably up to x_M ~0.2, but at x_M above 0.3, the fraction of the α-helix structure gradually increased with an increase in x_M. The fractions of turns and unordered structures did not change significantly with methanol content. Hence, the β-strand structure would change to the α-helix structure at x_M above 0.3.

In ethanol–water mixture, the change in the secondary structure of CI2 is qualitatively similar to that in methanol–water mixture. The maximum of β-strand content in ethanol–water mixture was found at ethanol mole fraction x_E ~ 0.05 which is lower than that in methanol–water mixture. Moreover, the

fraction of the α-helix structure rapidly increased with increasing x_E above ~0.15 and became almost independent of ethanol concentration at x_E above 0.45 in contrast with the case of methanol–water mixture. This result indicates that the structure of CI2 is denatured at $x_E \approx 0.45$. A similar trend was observed in the near-UV CD spectra of CI2 in ethanol–water mixture as a function of x_E (Fig. 3). The positive peak at 280 nm was assigned to tryptophan and thyrosine and decreased with increasing x_E. The molar ellipticity of CI2 at 280 nm was plotted against x_E and is shown in Fig. 4. In the figure, two breakpoints appear at $x_E \sim 0.2$ and 0.5. The result of the near-UV CD spectra is consistent with that of the far-UV CD spectra.

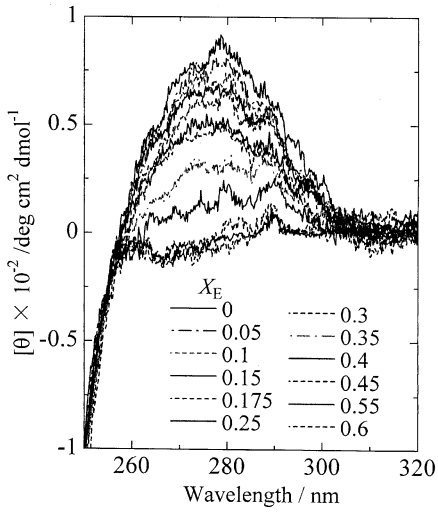

Fig. 3 Near-UV CD spectra of CI2 in aqueous mixtures of ethanol as a function of ethanol mole fraction.

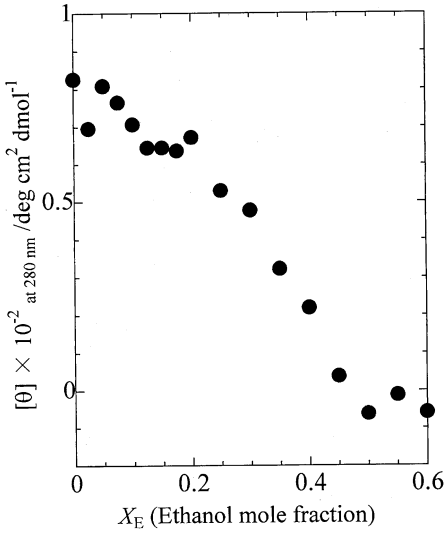

Fig. 4 The ellipticity of CI2 at a wavelength 280 nm as a function of ethanol mole fraction.

In TFE–water and HFIP–water mixtures, as seen in Figs. 1 and 2, the change in secondary structure to α-helix of CI2 took place at much smaller alcohol mole fractions than aqueous mixtures of methanol and ethanol. In Fig. 2, the maximum of β-strand structure was observed at TFE mole fraction $x_T \sim 0.01$ in TFE–water mixtures and at much smaller HFIP mole fraction (0.0085) in HFIP–water mixtures. The conversion to the α-helix structure of CI2 started at $x_{TFE} \sim 0.07$ and $x_{HFIP} \sim 0.01$ in aqueous mixtures of TFE and HFIP, respectively.

Summarizing the results of the far- and near-UV CD spectra of CI2 in the alcohol–water mixtures, it is concluded that α-helix formation of CI2 strongly depends on the nature of alcohols (i.e., solvent structures) in an order of HFIP > TFE > ethanol > methanol in effectiveness. Moreover, it should be noted that the structure transition of alcohol–water mixtures undergoes from ice-like network of water to chain-like zigzag structure of alcohols at ~0.3, ~0.2, ~0.2, and ~0.1 in aqueous mixtures of methanol, ethanol, TFE, and HFIP, respectively, in a similar order of HFIP > TFE > ethanol > methanol [12–18]. Thus, the solvent clusters do play an important role in α-helix formation of CI2 in aqueous mixtures of alcohols, as has been found for β-lactoglobulin and melittin [8].

SAXS and SANS spectra

The small-angle scattering data were analyzed by the conventional Guinier method. In the small-angle region, the scattering intensity $I(q)$ is approximated by

$$I(q) = I(0) \exp(-R_g^2 q^2/3)$$

where $I(0)$ is the scattering intensity at $q = 0$ and R_g is the radius of gyration. Figures 5 and 6 show the Guinier plots of the SAXS and SANS data, respectively, on CI2 in ethanol–water mixture at various mole fraction x_E. The least-squares fitting procedure was applied to the scattering data in a Guinier range ($R_g q < 1.3$); the values of R_g thus obtained are plotted against x_E in Fig. 7. The R_g values from

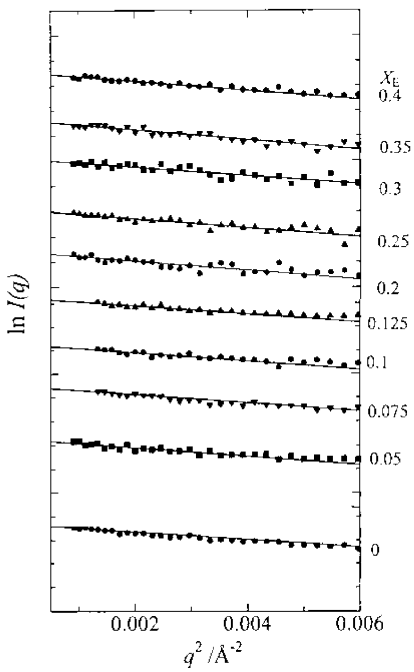

Fig. 5 Guinier plots of CI2 from the SAXS data in ethanol–water mixtures at various ethanol mole fractions x_E. Filled marks are experimental data, and the solid lines are fitted values.

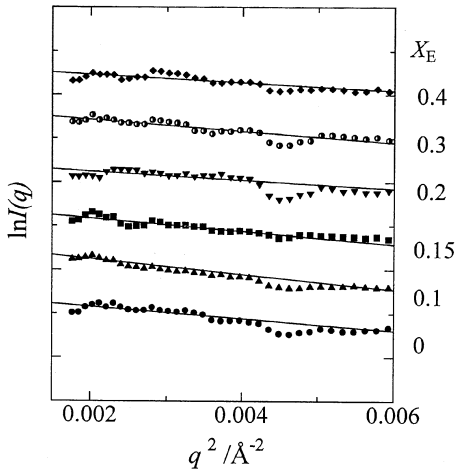

Fig. 6 Guinier plots of CI2 from the SANS data in ethanol–water mixtures at various ethanol mole fractions x_E. Filled marks are experimental data, and the solid lines are fitted values.

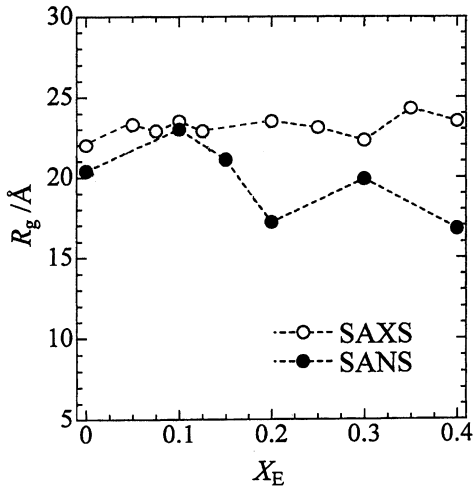

Fig. 7 The ethanol mole fraction dependence of R_g of CI2 in ethanol–water mixtures from SAXS and SANS.

both SAXS and SANS measurements slightly increased with an increase in x_E up to ~0.1, suggesting that the structure of CI2 in water is preserved, but swelled probably by ethanol entering inside CI2. With a further increase in x_E the values of R_g from SAXS did not change appreciably, whereas those from SANS significantly decreased.

To investigate the shape of CI2 in ethanol–water mixtures as a function of x_E, the Kratky method was applied to the SAXS data by plotting $q^2I(q)$ against q in Fig. 8. The same analysis was not made on the SANS data because of their insufficient quality of the data. As seen in the figure, in a range of $0 < x_E \leq 0.15$ there appeared a peak in a q-range of 0.1–0.2, whereas the figures show a monotonous increase in $q^2I(q)$ when x_E is above 0.2. This result suggests that CI2 changes its shape from globular to rod-like structure when x_E crosses ~0.15. This finding might be a hint to explain the different behavior in R_g from SAXS and SANS in Fig. 7. It should be noted that CI2 was measured in heavy water and its mixtures with fully deuterated ethanol by SANS to reduce background due to a huge incoherent scattering cross-section (80.27 barn) of hydrogen compared with that (2.05 barn) of deuterium. Thus, a

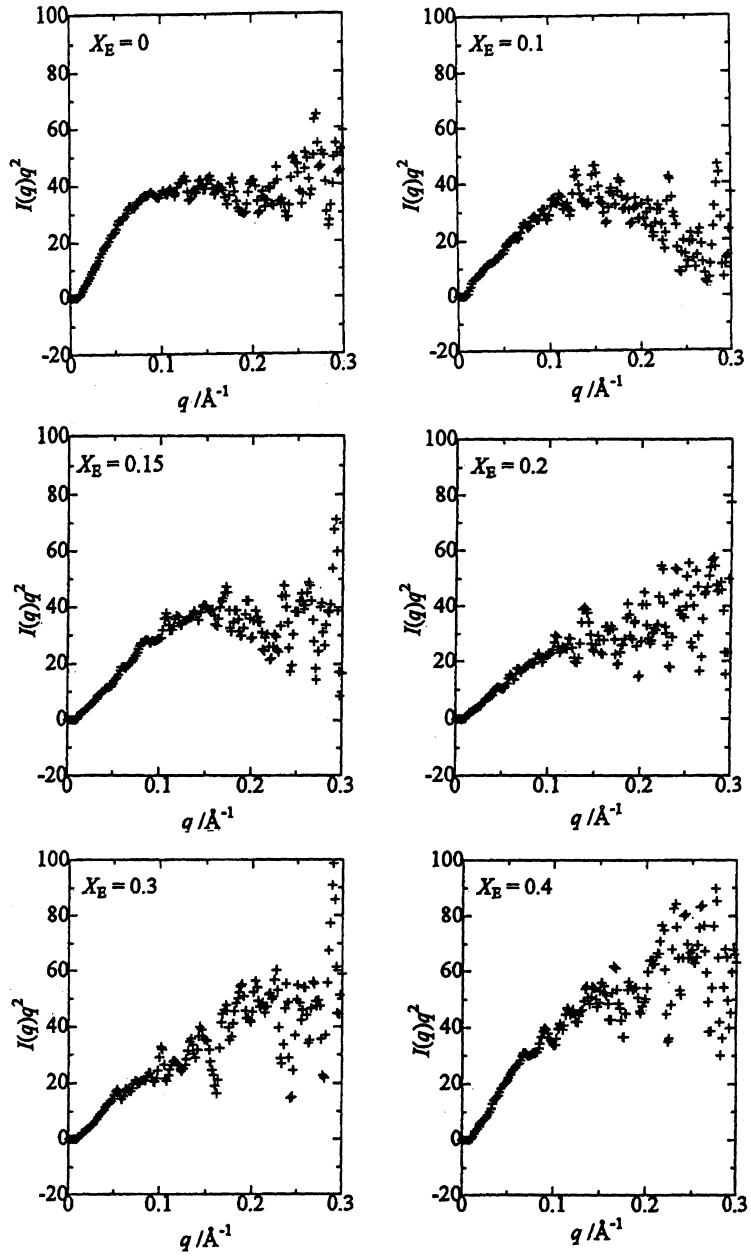

Fig. 8 Kratky plots of CI2 from the SAXS data in ethanol–water mixtures at selected ethanol mole fractions x_E.

contrast in scattering density between CI2 and solvent would decrease due to proton exchange between the exposed residues, which are embedded in CI2 in a globular state, and deuterated solvents in a denatured state at $x_E > 0.2$, resulting in the decrease in R_g when x_E is above 0.2.

DISCUSSION

We now discuss the plausible mechanism of alcohol-induced α-helix formation of protein in view of solvent structure. From a number of structural studies on alcohol–water mixtures [12–18] it has been

found that the structural transition takes place from the ice-like cluster of water to the chain-like one of alcohols with increasing alcohol concentration and that the alcohol concentration of the structural transition shifts to a water-rich region with lengthening and/or fluorination of the hydrophobic group of alcohols (i.e., HFIP > TFE > ethanol > methanol). This tendency is in good agreement with the order of alcohol-induced α-helix formation of CI2 in the corresponding alcohol–water mixtures. Figure 9 shows an example of three-dimensional structure of ethanol–water mixtures at ethanol mole fractions of 0.1, 0.2, and 0.4 obtained by NDIS and EPSR method [15]. As seen in the figure, the ice-like network of water remains at $x_E = 0.1$, but is broken down except for the nearest-neighbor pentamer unit at $x_E = 0.4$. On the other hand, at $x_E = 0.1$, ethanol molecules are assembled together to build up a micelle-like structure where the hydrophobic groups of ethanol forms a core with the hydroxyl groups hydrogen bonded with the surrounding water molecules. With increasing x_E to 0.4, the chain-like zigzag structure of ethanol is gradually formed. Here, it should be noted that the native state of CI2 is stable as long as the ice-like network of water remains in alcohol–water mixtures. In the REMD simulation result [11], a peptide forms hydrogen bonds with surrounding water molecules in water, whereas in ethanol the peptide tends to form internal hydrogen bonds, initiating α-helix formation in the peptide because of less hydrogen bonding between the peptide and solvent in ethanol than in water. These findings suggest that a balance in hydrogen-bonding probability between a protein–solvent and the protein–protein is essential in formation of α-helix in the protein. When the solvent environment of a protein is the ice-like network of water, the protein stabilizes such a secondary structure as the polar groups of the protein can form the hydrogen bonds with surrounding water molecules. On addition of alcohols into water so that the chain-like clusters of alcohols become predominant in the solution (i.e., after the structural transition of solvent clusters), the protein would tend to form the internal hydrogen bonds rather than hydrogen bonds with the surrounding alcohols since alcohols have much fewer sites for hydrogen bonding than water. In more concentrated alcohol solutions, the hydrophilic part of CI2 is no longer exposed to water because of lack of water. Under this condition, the hydrophilic groups of a protein tend to combine with each other, resulting in formation of the α-helix structure.

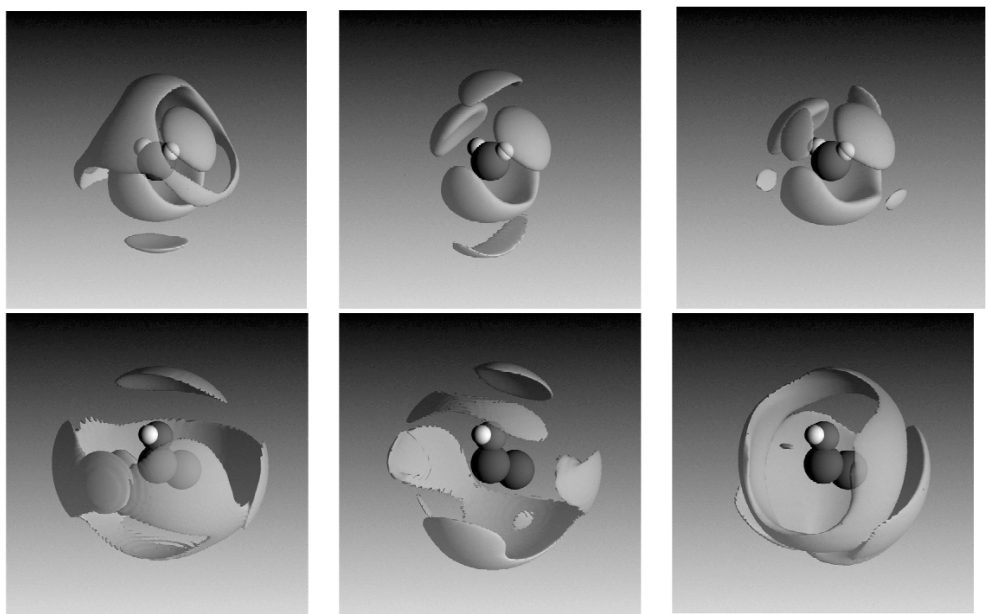

Fig. 9 Spatial density functions (SDFs) for ethanol–water mixtures [15]. The top three panels show the SDFs for water around a central water molecule at $x_E = 0.1$ (left), 0.2 (center), and 0.4 (right), and the bottom three panels show the corresponding SDFs for ethanol around an ethanol molecule, both from 2 to 7 Å.

ACKNOWLEDGMENTS

This study was partly supported by Grants-in-Aid for Scientific Research (15076211, 17550023, and 16GS0417) from MEXT and by MEXT.HAITEKU (2002-2006). This work was performed under the approval of the Photon Factory Program Advisory Committee (Proposal No. 99G128) and the KENS Program Advisory Committee (Proposal No. 99-B2-48).

REFERENCES

1. M. Buck. *Q. Rev. Biophys*. **31**, 297 (1998).
2. R. Rajan, P. Balaram. *Int. J. Pept. Protein Res*. **48**, 328 (1996).
3. M. Buck, H. Schwalbe, C. M. Dobson. *J. Mol. Biol*. **257**, 669 (1996).
4. H. Lu, M. Buck, S. E. Radford, C. M. Dobson. *J. Mol. Biol*. **265**, 112 (1997).
5. S. Kumaran, R. P. Roy. *J. Pept. Res*. **53**, 284 (1999).
5. F. Khan, R. H. Khan, S. Muzammil. *Biochim. Biophys. Acta* **1481**, 229 (2000).
6. R. Stoll, W. Voelter, T. A. Holak. *Biopolymers* **41**, 623 (1997).
7. N. Hirota-Nakaoka, Y. Goto. *Bioorg. Med. Chem*. **7**, 67 (1999).
8. D. Hong, M. Hoshino, R. Kuboi, Y. Goto. *J. Am. Chem. Soc*. **121**, 8427 (1999).
9. M. Kinoshita, Y. Okamoto, F. Hirata. *J. Am. Chem. Soc*. **122**, 2773 (2000).
10. M. Fioroni, M. D. Diaz, K. Burger, S. Berger. *J. Am. Chem. Soc*. **124**, 7737 (2002).
11. Y. Yoshida, T. Yamaguchi, Y. Okamoto. *Chem. Phys. Lett.* **412**, 280 (2005).
12. T. Takamuku, T. Yamaguchi, M. Asato, M. Matsumoto, N. Nishi. *Z. Naturforsch., A* **55**, 513 (2000).
13. M. Matsumoto, N. Nishi, T. Furusawa, M. Saita, T. Takamuku, M. Yamagami, T. Yamaguchi. *Bull. Chem. Soc. Jpn*. **68**, 1775 (1995).
14. N. Nishi, S. Takahashi, M. Matsumoto, A. Tanaka, K. Muraya, T. Takamuku, T. Yamaguchi. *J. Phys. Chem*. **99**, 462 (1995).
15. T. Yamaguchi, T. Takamuku, A. K. Soper. *J. Neutron Res.* **13**, 129 (2005).
16. T. Takamuku, T. Kumai, K. Yoshida, T. Otomo, T. Yamaguchi. *J. Phys. Chem. A* **109**, 7667 (2005).
17. K. Yoshida, T. Yamaguchi, T. Adachi, T. Otomo, D. Matsuo, T. Takamuku, N. Nishi. *J. Chem. Phys*. **119**, 6132 (2003).
18. K. Yoshida, T. Yamaguchi, D. T. Bowron, J. L. Finney. *J. Neutron Res*. **12**, 305 (2004).
19. G. M. Clore, A. M. Gronenborn, M. N. James, M. Kjaer, C. A. McPhalen, F. M. Poulsen. *Protein Eng.* **1**, 305 (1987).
20. G. M. Clore, A. M Gronenborn, M. Kjaer, F. M. Poulsen. *Protein Eng.* **1**, 313 (1987).
21. S. Ludvigsen, H. Y. Shen, M. Kjaer, J. C. Madsen, F. M. Poulsen. *J. Mol. Biol*. **222**, 621 (1991).
22. N. Sreerama, R. W. Woody. *Anal. Biochem*. **287**, 252 (2000) and refs. therein.